Pharm Res (2012) 29:490–499
DOI 10.1007/s11095-011-0578-3

RESEARCH PAPER

Subcutaneous Absorption of Monoclonal Antibodies: Role of Dose, Site of Injection, and Injection Volume on Rituximab Pharmacokinetics in Rats

Leonid Kagan • Michael R. Turner • Sathy V. Balu-Iyer • Donald E. Mager

Received: 3 June 2011 / Accepted: 22 August 2011 / Published online: 2 September 2011

ABSTRACT

Purpose To determine the effect of dose, the anatomical site of injection, and the injection volume on subcutaneous absorption of rituximab in rats and to explore absorption mechanisms using pharmacokinetic modeling.

Methods Rituximab serum concentrations were measured following intravenous and subcutaneous administration at the back, abdomen, and foot of rats. Several pharmacokinetic models were developed that included linear and saturable absorption, and degradation and/or protective binding at the injection site.

Results Rituximab exhibited linear kinetics following intravenous administration; however, bioavailability following subcutaneous injection was inversely related to the dose level. For the 1 mg/kg dose, bioavailability was approximately 70% at all tested injection sites, with faster absorption from the foot (T_{max} = 12 h for foot *vs.* 4.6 days for back). Bioavailability for the 10 mg/kg dose was 44 and 31% for the abdomen and back sites and 18% for 40 mg/kg injected at the back. A pharmacokinetic model that included binding as part of the absorption mechanism successfully captured the nonlinearities in rituximab absorption.

Conclusion The anatomical site of subcutaneous injection influences the rate of absorption and bioavailability of rituximab in rats. Saturable binding may be a major determinant of the nonlinear absorptive transport of monoclonal antibodies.

KEY WORDS lymphatic absorption · pharmacokinetic modeling · saturable absorption · therapeutic proteins

INTRODUCTION

The majority of marketed monoclonal antibodies (mAbs) are given intravenously and exhibit high water solubility, prolonged biological half-life and a relatively low risk of nonspecific toxicities (1). In contrast, subcutaneous (SC) injection is widely utilized in clinical practice for delivery of therapeutic macromolecules (such as hormones and cytokines). SC injection is more convenient and also provides extended delivery from a site of administration to the systemic circulation; thereby maintaining therapeutic drug concentrations for prolonged periods of time and reducing required dosing frequency. Challenges for this route of administration for mAbs include complex pharmacokinetics, higher incidence of immune response against the drug, and low or incomplete bioavailability following extravascular administration (2–5). Binding of antibody to its therapeutic target (via the Fab region) and/or Fc-mediated binding to immunoglobulin receptors (such as FcRn and/or FcγR) may also influence its pharmacokinetics (6,7).

SC injection is an approved route of administration for many therapeutic proteins, including several mAbs. The bioavailability of proteins following SC administration varies considerably, ranging from 12 to 100% (8,9), and the determinants of such variability are still unknown. The absolute bioavailability of mAbs ranges between 50 and 100% (3,10). Multiple factors can affect the rate and extent of protein SC absorption, such as size of the macromole-

Electronic Supplementary Material The online version of this article (doi:10.1007/s11095-011-0578-3) contains supplementary material, which is available to authorized users.

L. Kagan (✉)
Department of Pharmaceutical Sciences
University at Buffalo, State University of New York
363 Hochstetter Hall
Buffalo, New York 14260, USA
e-mail: lkagan@buffalo.edu

M. R. Turner • S. V. Balu-Iyer • D. E. Mager
Department of Pharmaceutical Sciences
University at Buffalo, State University of New York
Buffalo, New York 14260, USA

cule, formulation excipients, and application of pressure or heat (9,11,12). Studies conducted in sheep have identified the lymphatic system as a major absorption route for high molecular weight proteins (11,13,14). However, the lymphatic system contributes minimally to the overall bioavailability of SC administered proteins in rodents (15–17). Several preclinical and clinical studies have demonstrated that the anatomical site of SC injection can influence the bioavailability and rate of absorption of protein drugs, and there is no consensus for an optimal injection site (14,18–20). The rates of disappearance of liposomes from the injection site and lymphatic uptake are also significantly different between SC injections into the flank and foot of rats (21).

Proteolytic degradation at the site of injection has been proposed as a cause for incomplete bioavailability of proteins administered by SC injection (9,22). Parathyroid hormone and calcitonin bioavailabilities were improved by coadministration with aprotinin, a serine protease inhibitor (23). The SC bioavailability of interferon-β in monkeys appears to increase with dose, and saturation of site-specific metabolism was hypothesized to be a source of this phenomenon (24).

Distinct from other classes of therapeutic proteins and peptides, mAbs exhibit relatively greater molecular weight and circulating half-lives, and also utilize antibody-specific mechanisms (e.g., FcRn) to minimize proteolytic degradation. Whereas many studies have evaluated the SC absorption of hormones and cytokines, little is known regarding determinants of mAb absorption following SC injection. The first aim of this study is to investigate the effect of dose, the anatomical site of injection, and the injection volume on SC absorption of mAbs in rats. The second aim is to explore absorption mechanisms using pharmacokinetic modeling.

Rituximab, a chimeric murine/human mAb that reacts with the CD20 antigen expressed on the surface of normal and malignant human B-lymphocytes, was used as a model drug. It contains the light and heavy chain variable domains of the murine anti-CD20 antibody 2B8 in conjunction with human kappa and IgG1 heavy-chain constant region sequences (25). Rituximab shows efficacy in patients with various lymphoid malignancies, including B-cell non-Hodgkin's lymphoma and B-cell chronic lymphocytic leukaemia (26). Binding of mAbs to their antigenic target can affect their pharmacokinetics (6,27); therefore, selection of the rat model is advantageous, as normal rats do not express human CD20 antigen.

MATERIALS AND METHODS

Materials

Goat anti-human IgG (Fc specific)–peroxidase conjugate (A0170) and o-phenylenediamine (SigmaFast™ OPD, P9187) were obtained from Sigma-Aldrich, St. Louis, MO. Rat anti-rituximab monoclonal antibody was purchased from AbD Serotec, Raleigh, NC. Bovine serum albumin (BSA), phosphate buffered saline (PBS), carbonate-bicarbonate buffer, polysorbate 20 (Tween-20) and sulfuric acid were purchased from VWR, West Chester, PA.

Animals

Male Wistar rats, weighing 375–400 gr, were purchased from Harlan Laboratories Inc. (Indianapolis, IN). This study was conducted in accordance with an approved protocol by the Institutional Animal Use and Care Committee at the University at Buffalo, State University of New York. Two animals were housed in each cage during the study with free access to standard food and water and maintained on a 12/12 h light/dark cycle. Rats were allowed to acclimate for 1 week before study initiation.

Experimental Procedure

Animals were divided into ten groups (n=4–5 each) according to the route of administration, dose level, and injection volume (Table I). Animals were anaesthetized before drug administration using 5% isoflurane (IsoThesia™, Butler animal health supply, Dublin, OH). Three dose levels (1, 10, and 40 mg/kg) were evaluated, where each animal received a single dose by either intravenous (IV) or subcutaneous (SC) injection. For IV administration, rituximab was followed by 200 μL of normal saline to ensure delivery of the entire dose. SC injection was performed at the lower back, middle abdomen, or at the dorsal side of the left hind foot. IV and SC injection to

Table I Experimental Groups for Evaluating Rituximab Pharmacokinetics in Rats

Route	Site	Dose (mg/kg)	Injection volume (mL/kg)
IV	Tail vein	1	1 [a]
IV	Tail vein	10	1
SC	Back	1	1 [a]
SC	Back	10	1
SC	Back	40	4
SC	Back	10	4 [a]
SC	Abdomen	1	1 [a]
SC	Abdomen	10	1
SC	Foot	1	0.1
SC	Foot	1	0.3 [a]

[a] commercially available formulation (10 mg/mL) diluted with normal saline

the back and abdomen were performed using a 27 G needle, whereas a 31 G needle was used for injection to the foot. Commercially available rituximab (Rituxan®, 10 mg/mL; Genentech, Inc., San Francisco, CA) was diluted (when required) with sterile normal saline.

Serial blood samples (150 µL) were obtained following drug administration from the saphenous vein under isoflurane anesthesia using nonheparinized microhematocrit tubes (Fisherbrand®, Fisher Scientific, Pittsburgh, PA). For IV dosing groups, the sampling times were 10 min, 1, 2, 5, 11 h, and 1, 2, 4, 7, 10, 14 days, and then weekly for up to 8 weeks. For SC dosing groups, the sampling times were 1, 2, 5, 8, 11 h, and 1, 2, 3, 4, 7, 10, 14 days, and then weekly for up to 8 weeks. Blood was allowed to clot at room temperature for 30–60 min, and serum was separated by centrifugation at 2000 g for 20 min at 4°C. Serum was divided into aliquots and stored at −80°C until analysis.

Analytical Assay

A sandwich ELISA was used to quantify rituximab in rat serum samples, which was based on previously published methods (28,29) and modified to meet our requirements. This method is based on the chimeric nature of rituximab and utilizes two distinct antibodies for capture and detection of rituximab. Briefly, ELISA plates (F-bottom Maxisorp®, Nunc) were coated with 100 µL/well of anti-rituximab antibody solution (1 µg/mL in carbonate-bicarbonate buffer, pH 9.4, 0.2 M) overnight at 4°C. The rat IgG2a (clone MB2A4) specifically recognizes the idiotypic determinants expressed by rituximab. Between steps, wells were washed three times with 250 µL of a washing buffer (PBS + 0.05% Tween-20). All other incubations were performed at room temperature. Nonspecific binding was prevented by blocking plates for 1 h with 150 µL of PBS + 1% BSA. Samples and standards (100 µL) were incubated in duplicate for 1 h. For detection, goat anti-human IgG (Fc specific)–peroxidase conjugate (1:50,000 dilution in PBS, 100 µL) was added for 1 h; and plates were developed using 100 µL of freshly prepared OPD for 25 min in the dark. The reaction was stopped using 50 µL H_2SO_4 (1 M) and the optical density at 492 nm was measured within 10 min.

Samples were prepared at 1:100, 1:1,000, or 1:10,000 dilution using PBS + 1%BSA. Calibration curves were prepared by spiking corresponding standards into rat serum (5 µL into 95 µL of serum) and subsequent dilution using PBS + 1%BSA to match the dilution of the analyzed samples. Samples and standards were analyzed in duplicate. The working range of the assay was between 0.25 and 62.5 ng/mL. The calibration curves were successfully fitted with a four-parameter logistic equation. The precision was within ±10% and accuracy was within ±20%, which is in line with accepted recommendations for ligand binding assays (30,31). Dilutional linearity was confirmed during assay optimization.

Pharmacokinetic Model

Several pharmacokinetic models were compared to investigate the apparent nonlinear absorption of rituximab. Three competing processes are assumed to occur at the SC absorption site: systemic absorption, proteolytic degradation, and binding (most likely to FcRn) that can protect rituximab from degradation. The basic proposed model structures are shown in Fig. 1. Model A, reflects the hypothesis that binding to FcRn creates a depot that is protected form degradation, where only free rituximab can undergo presystemic elimination or be absorbed. In model B, the binding not only protects rituximab from degradation but is also responsible for drug absorption. Model C (Fig. 1) shows the structure of the final model, wherein drug administered at the injection site (A_{inj}) is transferred to an absorption site by a first-order process (k_{inj}). At the absorption site, free rituximab (ABS_{free}) can bind to a receptor (R) to form a complex ($DR = ABS_{tot} - ABS_{free}$), which was assumed to occur rapidly and characterized by the equilibrium dissociation constant (K_D). Free rituximab can undergo degradation or absorption by first-order processes (k_{deg} and k_{a1}). The drug-receptor complex delivers rituximab to the systemic circulation by a first-order process (k_{a2}). The amount of total receptor at the absorption site was assumed to remain constant with time, which is supported by extensive cellular recycling of FcRn (32,33). Systemic disposition of rituximab includes nonspecific distribution (A_t) and first-order elimination (k_{el}). The following equations were used to describe the final model:

$$\frac{dA_{inj}}{dt} = -k_{inj} \cdot A_{inj} \tag{1}$$

$$\frac{dABS_{tot}}{dt} = k_{inj} \cdot A_{inj} - (k_{deg} + k_{a1}) \cdot ABS_{free} - k_{a2} \cdot (ABS_{tot} - ABS_{free}) \tag{2}$$

$$ABS_{free} = 0.5 \cdot \left[(ABS_{tot} - R_{tot} - K_D) + \sqrt{(ABS_{tot} - R_{tot} - K_D)^2 + 4 \cdot K_D \cdot ABS_{tot}} \right] \tag{3}$$

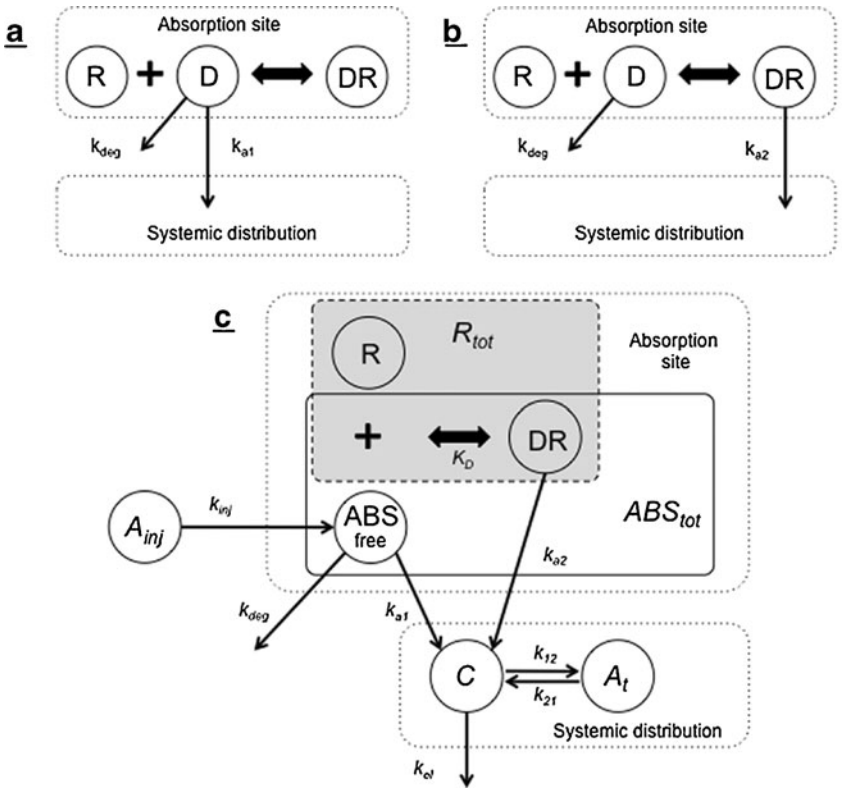

Fig. 1 Proposed model structures for rituximab pharmacokinetics in rats. Model **a** is based on degradation (k_{deg}) and absorption (k_{a1}) of free rituximab at the injection site. Model **b** is based on degradation (k_{deg}) of free rituximab and absorption of rituximab-receptor complex (k_{a2}). Model **c** is the final model used to describe rituximab absorption and disposition and includes absorption of both free rituximab and rituximab-receptor complex. D—free drug, R—free receptor, and DR—drug-receptor complex ($DR = ABS_{tot} - ABS_{free}$).

$$\frac{dC}{dt} = k_{a1} \cdot \frac{ABS_{free}}{V_c} + k_{a2} \cdot \frac{(ABS_{tot} - ABS_{free})}{V_c} - (k_{el} + k_{12}) \cdot C + k_{21} \cdot \frac{A_t}{V_c} \quad (4)$$

$$\frac{dA_t}{dt} = k_{12} \cdot C \cdot V_c - k_{21} \cdot A_t \quad (5)$$

where C is the rituximab concentration in the central compartment (with volume of V_c), A_t is the amount of rituximab in the peripheral distribution compartment, and k_{12} and k_{21} are the first-order transfer rate constants between central and peripheral compartments. For intravenous administration, $C(0)$ was set equal to Dose/V_c, and initial conditions for Eqs. 1, 2, and 5 were set to zero. For SC administration, $A_{inj}(0)$ was set equal to Dose, and initial conditions for Eqs. 2, 4, and 5 were set to zero.

Data Analysis

A standard noncompartmental data analysis was performed for each individual rituximab concentration-time profile. The maximum plasma drug concentration (C_{max}) and time to reach C_{max} (T_{max}) were obtained directly from the experimental data. Terminal half-life, area under the concentration time curve from time zero to infinity (AUC, calculated by linear trapezoidal method), mean residence time (MRT), volume of distribution at steady state (V_{ss}), and clearances were calculated. The bioavailability following SC administration was calculated by dividing individual AUC values by the mean AUC following IV administration of the same dose level. In addition, individual rituximab concentration-time profiles after IV injection were fitted using a biexponential equation. The mean estimated parameters were used to perform a deconvolution analysis of the pharmacokinetic profiles following SC administration. The noncompartmental analysis and deconvolution were performed using Phoenix™ WinNonlin® 6.1 (Pharsight, Mountain View, CA).

An ANOVA was applied to assess differences in pharmacokinetic parameters between more than two groups followed by a Tukey Multiple Comparisons Test where appropriate. Comparisons between two groups were conducted using the two tailed t-test. A p-value of less than 0.05 was considered statistically significant. Data are presented as mean ± SD, unless stated otherwise.

Initially, the data following intravenous administration were fitted separately and the estimated parameters (k_{el}, k_{12}, k_{21}, V_c) were fixed for the development of the absorption model. Several model structures for the absorption model

were evaluated using the data from three dose levels administered at the back and two dose levels administered at the abdomen. Finally, a simultaneous fitting of the model to all seven data sets was performed. As only one dose level was evaluated for the foot injection, the data from this site was excluded from model development. In addition, the pharmacokinetic profiles of rituximab following injection of 10 mg/kg at the back were similar, and only the profile from the 1 mL/kg injection was included in the analysis.

Model fitting and parameter estimation were performed using MATLAB R2008a (The MathWorks, Natick, MA) and the maximum likelihood method. The variance model was defined as:

$$VAR_i = (\sigma_1 + \sigma_2 \cdot Y(\theta, t_i))^2 \quad (6)$$

where VAR_i is the variance of the ith data point, σ_1 and σ_2 are the variance model parameters, and $Y(\theta, t_i)$ is the ith predicted value from the pharmacokinetic model. The goodness-of-fit was assessed by system convergence, Akaike Information Criterion, estimator criterion value for the maximum likelihood method, and visual inspection of residuals and fitted curves.

RESULTS

Mean serum concentration-time profiles of rituximab administered to rats intravenously, at dose levels of 1 and 10 mg/kg, are presented in Fig. 2, and the corresponding pharmacokinetic parameters obtained by noncompartmental analysis are listed in Table II. Both dose levels demonstrated a polyexponential decrease in pharmacokinetic profiles (Fig. 2). For several rats, a slightly greater serum concentration was measured at 1 h compared with

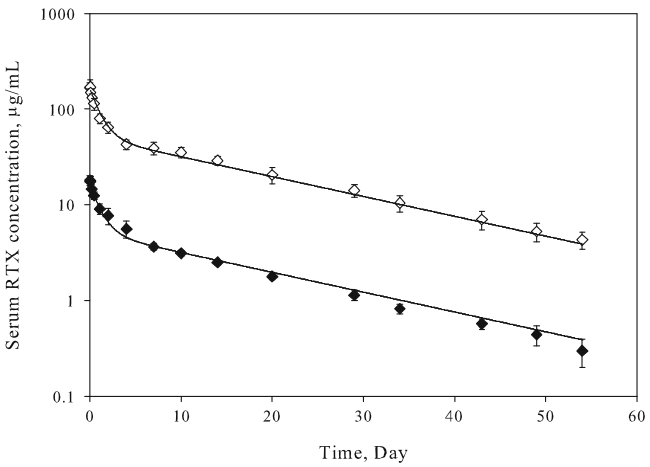

Fig. 2 Time-course of serum rituximab in rats following intravenous bolus administration. Symbols represent mean measured concentrations (♦—1 mg/kg and ◊—10 mg/kg), lines are model fitted profiles, and error bars represent S.D. ($n = 4$).

Table II Pharmacokinetic Parameters of Rituximab Following IV Administration to Rats Calculated by Noncompartmental Analysis

Parameter	Units	IV 1 mg/kg		IV 10 mg/kg	
		Mean	SD	Mean	SD
AUC	µg·Day/mL	118	12.0	1255	154
CL	mL/Day/kg	8.5	0.8	8.1	1.0
V_{ss}	mL/kg	141.2	23.3	155.4	14.6
$T_{1/2}$	Day	13.9	3.3	14.7	0.9
MRT	Day	16.6	2.6	19.4	1.2

AUC area under the plasma concentration-time curve; *CL* clearance; $T_{1/2}$ terminal half-life; *MRT* mean residence time; V_{ss} steady-state volume of distribution

that at 10 min. The reason for this finding is not clear, and it might be related to delayed distribution of rituximab from a peripheral vein to the systemic circulation. The terminal half-life of rituximab was approximately 2 weeks. Dose-normalized AUC and C_{max} values were not statistically different between groups, indicating linear pharmacokinetics at the tested dose range.

Mean serum concentration-time profiles of rituximab injected SC at the back (1, 10, and 40 mg/kg) and abdomen (1 and 10 mg/kg) regions are presented in Fig. 3. The corresponding values for bioavailability, C_{max} and T_{max} are shown in Fig. 4 (the full list of pharmacokinetic parameters obtained by noncompartmental analysis can be found in the online supplemental file). The extent of absorption, following injection at the back, decreased with increasing dose levels. For the 10 mg/kg dose, there was no statistical difference between two tested groups (back 1 and 4 mL/kg, t-test). However, injection of the same dose at a 4-fold higher volume (back 4 mL/kg) showed a trend toward a slightly greater bioavailability as compared to the 1 mL/kg injection. Similar to injections at the back, the bioavailability at the abdomen was dose-dependent, with higher bioavailability at the low dose. For the 10 mg/kg dose (1 mL/kg), the serum concentrations were statistically different from concentrations following injection at the back (for the same injection volume) from 2 h up to 21 days (with exception of Day 7). This resulted in a significantly higher bioavailability for abdominal injection as compared to injection at the back (43.7 *vs.* 31.2%).

The overall bioavailability of rituximab following SC injection (1 mg/kg) at the back, abdomen, and at the foot of rats was similar (Fig. 4). In contrast, the initial absorption behavior was different between groups (Fig. 5). C_{max} was attained as early as 12 h following injection at the foot as compared to 1.5 days following injection at the abdomen, and more than 4 days for injection at the back (Fig. 5a). For the foot site, there was a slight trend toward

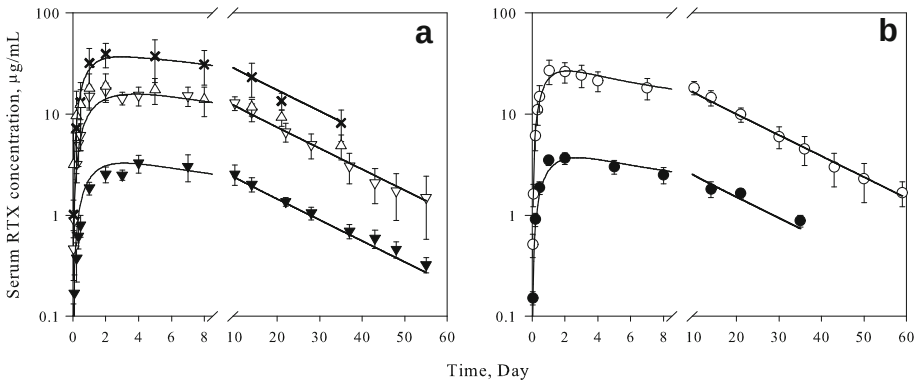

Fig. 3 Time-course of serum rituximab in rats following SC administration at the back (**a**) and abdomen (**b**). Symbols represent mean measured concentrations for injections at the back (▼—1 mg/kg, ∇—10 mg/kg (1 mL/kg), ▵—10 mg/kg (4 mL/kg), and **x**—40 mg/kg) and abdomen (●—1 mg/kg, ○—10 mg/kg). Lines are model fitted profiles, and error bars represent S.D. ($n = 4$–5).

greater initial concentrations following administration of a greater volume. Differences in AUC values over the first 7 days, which can serve as cumulative measurements for the initial absorption phase, are not reflected in the overall AUC values owing to the relatively long terminal half-life (Fig. 5b).

The majority of drug absorption following SC injection was completed within 7–10 days according to the deconvolution analysis (Fig. 6). The initial absorption rate was higher from the abdominal site as compared to the back. In addition, for both the abdomen and the back, the extent of absorption was dose-proportional (for 1 and 10 mg/kg doses) during the first two days following drug administration.

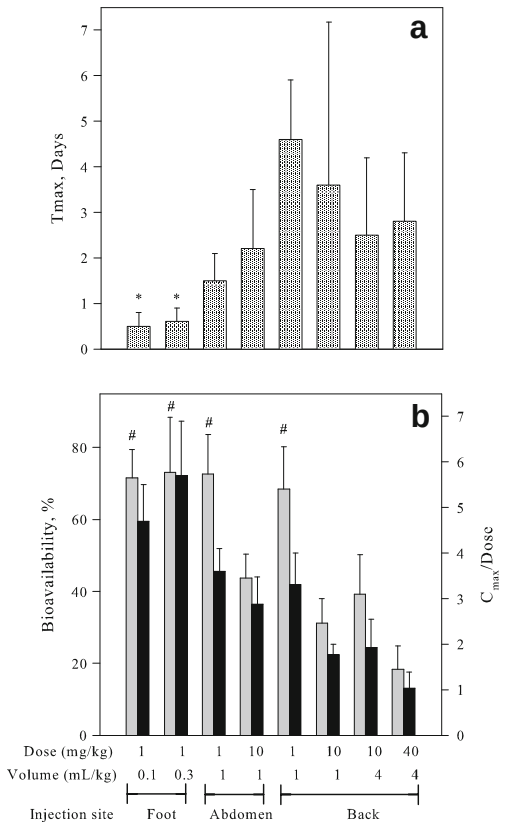

Fig. 4 Pharmacokinetic parameters calculated for rituximab administered by SC injection to rats by noncompartmental analysis. (**a**) T_{max} and (**b**) bioavailability (grey bars) and dose normalized C_{max} (black bars). *—significantly different from injection at the back ($p < 0.05$). #—significantly different from injection of 10 and 40 mg/kg ($p < 0.05$).

Pharmacokinetic modeling was used to investigate the mechanism(s) of absorption of rituximab following SC administration. A two-compartmental model with linear elimination provided a good description of the pharmacokinetic profiles following IV administration of both dose levels (Fig. 2). Model A was unable to describe the experimental data following SC administration (data not shown). Model B reasonably captured the dose-dependent SC bioavailability of rituximab; however, it resulted in an overprediction of concentrations for the highest dose level and an underprediction for the lowest dose level (data not shown). Therefore, Model C was constructed to include both absorption of the free drug as well as absorption of the drug-receptor complex. In addition, separation of the injection site from the absorption site resulted in a significant decrease in the objective function. The final model resulted in a good simultaneous description of the experimental data (Figs. 2 and 3). The estimated pharmacokinetic parameters are reported in Table III. Other models that were evaluated included first-order absorption kinetics from the injection site (A_{inj}) directly to the central compartment (C) or one that incorporated a Michaelis-Menten type saturable transport from the absorption compartment (ABS) to the central compartment (C). These models resulted in poorer fits and higher objective function values. A parameter for the injection volume was not included in the model, as this factor did not have a statistically significant impact on the bioavailability.

DISCUSSION

The rate and the extent of systemic uptake of mAbs following SC injection are governed by a complex interplay

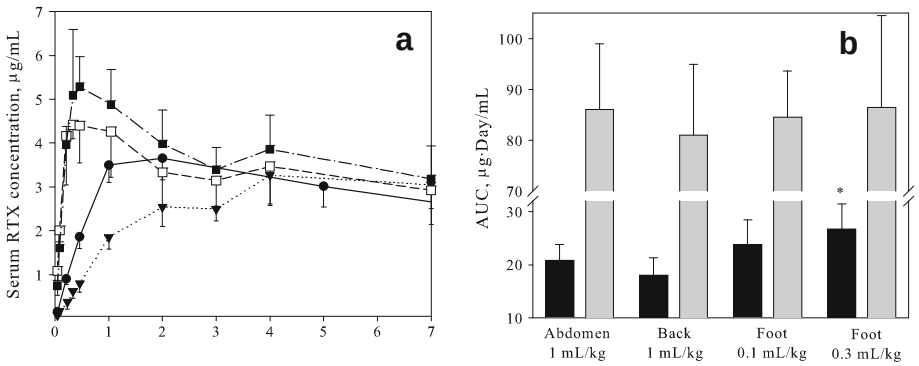

Fig. 5 Time-course of serum rituximab in rats following SC administration (1 mg/kg). The symbols are mean measured concentrations (▼—back, ●—abdomen, □—foot (0.1 mL/kg), and ■—foot (0.3 mL/kg)). (**a**) First 7 days after administration (linear plot). (**b**) AUC up to Day 7 (black bars) and for the full time-course (grey bars). Error bars represent S.D. ($n = 4$–5). *—significantly different from injection at the back ($p < 0.05$).

of several kinetic processes, including transport through the extracellular matrix, uptake by the blood and lymphatic capillaries, and presystemic elimination. Diffusion across the interstitium is likely dictated by molecular size and physical and electrostatic interaction with the various components of the interstitium (e.g., fibrous collagen network and glycosaminoglycanes) (9,34). Therefore, diffusion of large macromolecules through the interstitium would be significantly restricted.

Systemic absorption from the interstitial space can occur through either blood or lymphatic vessels that differ considerably in structure and physiology. The well-organized structure of blood capillaries poses a significant barrier for penetration of large hydrophilic molecules, such as proteins. Lymph is formed as interstitial fluid enters initial lymphatics, and a hydrostatic pressure gradient is considered as the main force causing lymphatic filling (34). The lack of tight junctions between the cells of the lymphatic capillaries allows for a relatively unhindered uptake of molecules from the interstitium. Resistance to fluid flow inside the lymphatics is lower than that in the extracellular matrix; therefore, it has been proposed that transport of macromolecules across the interstitium would be a rate-limiting step in their lymphatic absorption (34). Importantly, lymphatic absorption is a passive process that occurs as lymph is formed inside the tissues. As such, lymphatic uptake alone cannot explain the saturable absorption behavior that was observed for rituximab in this study.

A positive correlation exists between the molecular weight of protein drugs and the percent of the dose that is taken up by the lymphatics in sheep (35). According to these studies, mAbs should be absorbed almost exclusively by the lymphatic system. Uptake into regional lymph nodes following SC injection into hind foot pads of mice has been directly demonstrated using radiolabeled antibodies (36,37); however, the full-time course and drug bioavailability were not investigated. In contrast to studies in sheep, the lymphatic system does not significantly contribute to systemic protein absorption following SC administration in rodents (15–17). Harrell and coworkers concluded that lymphatic drainage of the flank and back areas are less

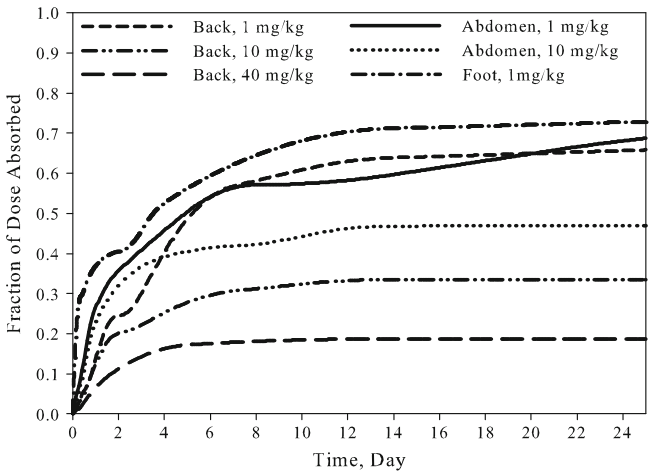

Fig. 6 Mean deconvolution profiles of rituximab in rats following SC administration.

Table III Final Estimated Pharmacokinetic Model Parameters

Parameter	Units	Mean	%CV[a]
V_c	L/kg	$6.10 \cdot 10^{-2}$	4
k_{12}	Day^{-1}	0.479	11
k_{21}	Day^{-1}	0.305	10
k_{el}	Day^{-1}	0.137	4
k_{deg}	Day^{-1}	0.513	9
R_{tot}	nmol/kg	10.9	16
K_D	nmol	3.00	18
k_{inj}	Day^{-1}	39.9	15
k_{a2}	Day^{-1}	0.295	8
k_{a1} back	Day^{-1}	$6.30 \cdot 10^{-2}$	8
k_{a1} abdomen	Day^{-1}	0.205	8

[a] Coefficient of variation of the estimate; does not reflect inter-animal variability

efficient than that of the limbs in mice (38). Both preclinical and clinical research has demonstrated that the anatomical site of SC injection may influence the rate and extent of absorption (14,18–20). One hypothesis is that the contribution of lymphatic and blood capillaries to the overall absorption might be dependent on the site of injection.

In this study, the SC absorption of rituximab was evaluated from three different injection sites. SC injection at the back is commonly utilized in rodents, and this site can accommodate large injection volumes due to large mobility of the skin. Injection at the foot has been utilized in many lymphatic absorption experiments, whereas the available SC space is much more limited at this site. Finally, the abdomen was selected as an injection site with intermediate characteristics. For the 10 mg/kg dose administered in the same volume, the bioavailability was significantly higher for abdominal injection as compared to injection at the back (43.7 *vs.* 31.2%). For the low dose, the absorption from the foot was faster than from the back or the abdomen. In addition, serum AUC (from time zero to day 7) after the foot injection (0.3 mL/kg) was approximately 150 % of the AUC following injection at the back (Fig. 5b). This initial difference is obscured by a very long terminal half-life and interanimal variability, resulting in no significant differences in total bioavailability between sites for the low dose (68.5 to 73.1%).

Faster absorption from the foot injection might be attributed to the facilitation of lymph formation and uptake by the injection. At the foot, injection of the lowest volume of 0.1 mL/kg resulted in a small bubble under the skin that was visually evident for at least 8 h post-injection and probably resulted in a significant elevated hydrostatic pressure at the injection site. On the other hand, injection of much larger volumes at the back (up to 4 mL/kg) can be accommodated by rats without significant elevation in pressure in surrounding tissues. This is supported by the trend for enhanced absorption following injection of higher volumes. We propose that the site of SC injection and the injection volume might have a greater impact on the pharmacokinetics of protein drugs with a shorter half-life and this hypothesis should be further investigated.

FcRn consists of two subunits (β2-microglobulin and MHC class I α chain) and binds IgG in a pH-dependent manner (39), which provides antibodies with protection from lysosomal catabolism. Binding to FcRn plays an important role in prolongation of the half-lives of circulating IgG (40,41). For example, the clearance of 7E3 (IgG1) in FcRn knockout mice is approximately 10-fold higher as compared to wild type animals (33). Furthermore, co-administration of 7E3 with a high dose of IVIG can lead to a saturation of this protective mechanism and increase the clearance of mAbs in wild type mice. In this study, the pharmacokinetics of rituximab in rats was linear (at the tested dose range, 1–10 mg/kg) following intravenous administration, and there was no evidence of saturation of the FcRn related binding at the systemic level. In contrast, the SC administration of rituximab resulted in dose-dependent pharmacokinetics. The bioavailability decreased with an increase in dose for both the back and the abdomen injection sites. This phenomenon might be due to saturation of protective binding at the injection site, producing a more efficient presystemic degradation at higher doses. The findings of this study are consistent with observations that the bioavailability of 7E3 following SC injection is approximately three times greater in wild type as compared to FcRn-deficient mice (42). Therefore, saturation of FcRn-mediated protection of mAbs from proteolytic degradation at the site of injection is a plausible explanation for dose-dependent absorption of rituximab in rats.

It has been proposed that the FcRn effect on SC bioavailability of mAbs could be related to binding-related protection from degradation or binding-mediated transport from the interstitial space to the blood (42). FcRn-mediated transport of IgG across cell has been demonstrated *in vitro* (43,44). In this study, pharmacokinetic modeling was used to help distinguish between these proposed mechanisms. Only models B and C that incorporated binding as a part of the absorption mechanism, as well as a degradation protection mechanism, were able to capture the observed dose-dependent bioavailability. The first-order absorption rate constant (k_{a1}) might be attributed to the lymphatic uptake of rituximab. Modeling revealed that utilization of injection site-specific parameters for this process was required to simultaneously capture the data from two absorption sites (back and abdomen). The developed model assumed rapid equilibrium between free and receptor-bound rituximab, which is mathematically consistent with previously published models (45,46). The model of drug binding at the absorption site was parameterized in units of amount (nmol), and the volume of the absorption site could not be estimated from the available data. Therefore, a direct comparison between estimated values of K_D and R_{tot} and reported information on rituximab binding to FcRn is not possible.

This study identified several factors that influence the absorption of rituximab in rats. Specific binding of rituximab to FcRn is assumed to play an important part of the absorption mechanism; however, this should be tested experimentally in future studies. Nevertheless, it can be further hypothesized that absorption of other antibodies (and Fc-fusion proteins) might depend on their affinity to FcRn. Interspecies differences in antibody-receptor interactions should also be considered (47). Species differences in the structure of the SC space

(48) also makes a direct projection of the results of this study to humans impractical. For example, the absorption of golimumab appears similar from three evaluated sites of injection (upper arm, abdomen, and thigh) (49). Future research is required to identify the best species and most relevant injection sites for preclinical assessment of SC absorption of proteins.

In conclusion, mechanisms of rituximab absorption in rats were evaluated following SC administration. The bioavailability of rituximab following SC injection in rats was inversely related to the dose level, which might be attributed to saturation of FcRn-mediated protective binding at the absorption site. The anatomical site of SC injection affects the rate and extent of absorption, and details of the SC injection site should be included in pharmacokinetic reports for mAbs and possibly other protein drugs. The volume of SC injection did not have a significant impact on rituximab pharmacokinetics. Modeling results suggest that binding (likely to FcRn) is an important determinant of the absorptive kinetics of mAbs following SC administration.

ACKNOWLEDGMENTS & DISCLOSURES

We thank Dr. John M. Harrold for his help in developing the MATLAB code for this project. Partial results of this study were presented at the 12th Buffalo Pharmaceutics Symposium in Buffalo, NY. This work was supported by the Center for Protein Therapeutics, University at Buffalo, SUNY.

REFERENCES

1. Roskos LK, Davis CG, Schwab GM. The clinical pharmacology of therapeutic monoclonal antibodies. Drug Develop Res. 2004;61:108–20.
2. Lin JH. Pharmacokinetics of biotech drugs: peptides, proteins and monoclonal antibodies. Curr Drug Metab. 2009;10:661–91.
3. Lobo ED, Hansen RJ, Balthasar JP. Antibody pharmacokinetics and pharmacodynamics. J Pharmaceut Sci. 2004;93:2645–68.
4. Tabrizi MA, Tseng CM, Roskos LK. Elimination mechanisms of therapeutic monoclonal antibodies. Drug Discov Today. 2006;11:81–8.
5. Ternantand D, Paintaud G. Pharmacokinetics and concentration-effect relationships of therapeutic monoclonal antibodies and fusion proteins. Expert Opin Biol Th. 2005;5:S37–47.
6. Dayde D, Ternant D, Ohresser M, Lerondel S, Pesnel S, Watier H, *et al.* Tumor burden influences exposure and response to rituximab: pharmacokinetic-pharmacodynamic modeling using a syngeneic bioluminescent murine model expressing human CD20. Blood. 2009;113:3765–72.
7. Urva SR, Yang VC, Balthasar JP. Physiologically based pharmacokinetic model for T84.66: A monoclonal anti-CEA antibody. J Pharmaceut Sci. 2010;99:1582–600.
8. Tang L, Persky AM, Hochhaus G, Meibohm B. Pharmacokinetic aspects of biotechnology products. J Pharm Sci. 2004;93:2184–204.
9. Porter CJ, Charman SA. Lymphatic transport of proteins after subcutaneous administration. J Pharm Sci. 2000;89:297–310.
10. Dirks NL, Meibohm B. Population pharmacokinetics of therapeutic monoclonal antibodies. Clin Pharmacokinet. 2010;49:633–59.
11. McLennan DN, Porter CJ, Edwards GA, Heatherington AC, Martin SW, Charman SA. The absorption of darbepoetin alfa occurs predominantly via the lymphatics following subcutaneous administration to sheep. Pharm Res. 2006;23:2060–6.
12. Porter CJ, Edwards GA, Charman SA. Lymphatic transport of proteins after s.c. injection: implications of animal model selection. Adv Drug Deliv Rev. 2001;50:157–71.
13. Charman SA, McLennan DN, Edwards GA, Porter CJ. Lymphatic absorption is a significant contributor to the subcutaneous bioavailability of insulin in a sheep model. Pharm Res. 2001;18:1620–6.
14. Kota J, Machavaram KK, McLennan DN, Edwards GA, Porter CJ, Charman SA. Lymphatic absorption of subcutaneously administered proteins: influence of different injection sites on the absorption of darbepoetin alfa using a sheep model. Drug Metab Dispos. 2007;35:2211–7.
15. Kagan L, Gershkovich P, Mendelman A, Amsili S, Ezov N, Hoffman A. The role of the lymphatic system in subcutaneous absorption of macromolecules in the rat model. Eur J Pharm Biopharm. 2007;67:759–65.
16. Kojima M, Hosoda H, Date Y, Nakazato M, Matsuo H, Kangawa K. Ghrelin is a growth-hormone-releasing acylated peptide from stomach. Nature. 1999;402:656–60.
17. Bocci V, Muscettola M, Grasso G, Magyar Z, Naldini A, Szabo G. The lymphatic route. 1) Albumin and hyaluronidase modify the normal distribution of interferon in lymph and plasma. Experientia. 1986;42:432–3.
18. Beshyah SA, Anyaoku V, Niththyananthan R, Sharp P, Johnston DG. The effect of subcutaneous injection site on absorption of human growth hormone: abdomen *versus* thigh. Clin Endocrinol (Oxf). 1991;35:409–12.
19. Macdougall IC, Jones JM, Robinson MI, Miles JB, Coles GA, Williams JD. Subcutaneous erythropoietin therapy: comparison of three different sites of injection. Contrib Nephrol. 1991;88:152–6. discussion 157–158.
20. Ter Braak E, Woodworth J, Bianchi R, Cerimele B, Erkelens D, Thijssen J, *et al.* Injection site effects on the pharmacokinetics and glucodynamics of insulin lispro and regular insulin. Diabetes Care. 1996;19:1437–40.
21. Oussoren C, Zuidema J, Crommelin DJA, Storm G. Lymphatic uptake and biodistribution of liposomes after subcutaneous injection I. Influence of the anatomical site of injection. J Liposome Res. 1997;7:85–99.
22. Lee VH. Enzymatic barriers to peptide and protein absorption. Crit Rev Ther Drug Carrier Syst. 1988;5:69–97.
23. Parsons JA, Rafferty B, Stevenson RW, Zanelli JM. Evidence that protease inhibitors reduce the degradation of parathyroid hormone and calcitonin injected subcutaneously. Br J Pharmacol. 1979;66:25–32.
24. Mager DE, Neuteboom B, Efthymiopoulos C, Munafo A, Jusko WJ. Receptor-mediated pharmacokinetics and pharmacodynamics of interferon-beta1a in monkeys. J Pharmacol Exp Ther. 2003;306:262–70.
25. Reff ME, Carner K, Chambers KS, Chinn PC, Leonard JE, Raab R, *et al.* Depletion of B cells *in vivo* by a chimeric mouse human monoclonal antibody to CD20. Blood. 1994;83:435–45.
26. Plosker GL, Figgitt DP. Rituximab: a review of its use in non-Hodgkin's lymphoma and chronic lymphocytic leukaemia. Drugs. 2003;63:803–43.
27. Davis CB, Bugelski PJ. Subcutaneous bioavailability of a PRIMATIZED IgG1 anti-human CD4 monoclonal antibody is dose dependent in transgenic mice bearing human CD4. Drug Deliv. 1998;5:95–100.

28. Beum PV, Kennedy AD, Taylor RP. Three new assays for rituximab based on its immunological activity or antigenic properties: analyses of sera and plasmas of RTX-treated patients with chronic lymphocytic leukemia and other B cell lymphomas. J Immunol Methods. 2004;289:97–109.
29. Blasco H, Lalmanach G, Godat E, Maurel MC, Canepa S, Belghazi M, *et al.* Evaluation of a peptide ELISA for the detection of rituximab in serum. J Immunol Methods. 2007;325:127–39.
30. DeSilva B, Smith W, Weiner R, Kelley M, Smolec J, Lee B, *et al.* Recommendations for the bioanalytical method validation of ligand-binding assays to support pharmacokinetic assessments of macromolecules. Pharm Res. 2003;20:1885–900.
31. Findlay JW, Dillard RF. Appropriate calibration curve fitting in ligand binding assays. AAPS J. 2007;9:E260–7.
32. Ober RJ, Martinez C, Vaccaro C, Zhou J, Ward ES. Visualizing the site and dynamics of IgG salvage by the MHC class I-related receptor, FcRn. J Immunol. 2004;172:2021–9.
33. Garg A, Balthasar JP. Physiologically-based pharmacokinetic (PBPK) model to predict IgG tissue kinetics in wild-type and FcRn-knockout mice. J Pharmacokinet Pharmacodyn. 2007;34:687–709.
34. Swartz MA. The physiology of the lymphatic system. Adv Drug Deliv Rev. 2001;50:3–20.
35. McLennan DN, Porter CJH, Charman SA. Subcutaneous drug delivery and the role of the lymphatics. Drug Discov Today: Tech. 2005;2:89–96.
36. Weinstein JN, Parker RJ, Keenan AM, Dower SK, Morse 3rd HC, Sieber SM. Monoclonal anitbodies in the lymphatics: toward the diagnosis and therapy of tumor metastases. Science. 1982;218:1334–7.
37. Steller MA, Parker RJ, Covell DG, Holton 3rd OD, Keenan AM, Sieber SM, *et al.* Optimization of monoclonal antibody delivery via the lymphatics: the dose dependence. Cancer Res. 1986;46:1830–4.
38. Harrell MI, Iritani BM, Ruddell A. Lymph node mapping in the mouse. J Immunol Meth. 2008;332:170–4.
39. Raghavan M, Bjorkman PJ. Fc receptors and their interactions with immunoglobulins. Annu Rev Cell Dev Biol. 1996;12:181–220.
40. Ghetie V, Hubbard JG, Kim JK, Tsen MF, Lee Y, Ward ES. Abnormally short serum half-lives of IgG in beta 2-microglobulin-deficient mice. Eur J Immunol. 1996;26:690–6.
41. Junghans RP, Anderson CL. The protection receptor for IgG catabolism is the beta2-microglobulin-containing neonatal intestinal transport receptor. Proc Natl Acad Sci U S A. 1996;93:5512–6.
42. Wang W, Wang EQ, Balthasar JP. Monoclonal antibody pharmacokinetics and pharmacodynamics. Clin Pharmacol Ther. 2008;84:548–58.
43. Dickinson BL, Badizadegan K, Wu Z, Ahouse JC, Zhu X, Simister NE, *et al.* Bidirectional FcRn-dependent IgG transport in a polarized human intestinal epithelial cell line. J Clin Invest. 1999;104:903–11.
44. Antohe F, Radulescu L, Gafencu A, Ghetie V, Simionescu M. Expression of functionally active FcRn and the differentiated bidirectional transport of IgG in human placental endothelial cells. Hum Immunol. 2001;62:93–105.
45. Hansen RJ, Balthasar JP. Pharmacokinetic/pharmacodynamic modeling of the effects of intravenous immunoglobulin on the disposition of antiplatelet antibodies in a rat model of immune thrombocytopenia. J Pharm Sci. 2003;92:1206–15.
46. Mager DE, Krzyzanski W. Quasi-equilibrium pharmacokinetic model for drugs exhibiting target-mediated drug disposition. Pharm Res. 2005;22:1589–96.
47. Ober RJ, Radu CG, Ghetie V, Ward ES. Differences in promiscuity for antibody-FcRn interactions across species: implications for therapeutic antibodies. Int Immunol. 2001;13:1551–9.
48. McDonald TA, Zepeda ML, Tomlinson MJ, Bee WH, Ivens IA. Subcutaneous administration of biotherapeutics: current experience in animal models. Curr Opin Mol Ther. 2010;12:461–70.
49. Xu Z, Wang Q, Zhuang Y, Frederick B, Yan H, Bouman-Thio E, *et al.* Subcutaneous bioavailability of golimumab at 3 different injection sites in healthy subjects. J Clin Pharmacol. 2010;50:276–84.